# Comparative Characterization of *in vivo* and *in vitro* Noise of the SIROF Utah Electrode Array

A. Tye Gardner[1], John Mize[2], David J. Warren[2], Ross M. Walker[1]
Departments of Electrical and Computer Engineering[1] and Bioengineering[2], University of Utah, Salt Lake City, USA

***Abstract*—Microelectrode arrays are one of the most important tools for advancing our knowledge of biological neural systems. Thorough characterization of microelectrode arrays helps designers optimize neural interface circuits and systems as well as microelectrodes themselves, which in turn enables a better understanding of nervous systems. Noise and impedance of electrode arrays are important for determining specifications for neural interface electronics, but data are largely lacking in the literature. This work presents engineering-oriented characterizations of the commonly used SIROF Utah Electrode Array. The study demonstrates a strong correlation between noise and impedance, and finds a significant increase in both noise and impedance *in vivo* versus *in vitro*. We also observe an increase in low-frequency (< 1 kHz) noise *in vivo* that is consistent with biological noise reported elsewhere.**

***Keywords—Utah Electrode Array, neural interface, neural amplifier, electrode impedance, electrode noise, in vivo noise***

## I. Introduction

Microelectrode array research has seen vast growth over recent years, providing tools at the leading edge of neuroscience, bioengineering and implanted medical devices that provide treatment for a range of medical challenges. The standard Utah Electrode Array (UEA) is a commonly used device in animal neuroscience and human neural prosthetic translational efforts [1][2], and is comprised of 400 µm pitch electrodes with 1.5 mm long shanks. These devices provide sensing interfaces to the nervous system with high spatial and temporal resolution (single cell activity), but experience high impedance and significant noise. High impedance of the electrode combined with the cumulative noise of the recording electronics, tissue, and background noise of nearby neurons reduces the number of detectable single neuron action potentials. Thorough characterization of these devices is part of the critical path forward in designing better neural interface circuits as well as understanding failure modes for long term implants.

Noise and impedance are critical and fundamental characteristics of electrodes. While single-frequency impedance data is generally available in the literature (1 kHz), full spectrum noise and impedance data are scarce and incomplete. While there have been several studies on microelectrode impedance characteristics [3] and several noise modeling studies related to other types of electrodes [4], our work contributes a thorough characterization of the correlation between spectral noise and impedance for the UEA [5]. Our previous work was limited to *in vitro* testing in saline solution, but demonstrated that impedance measurements could accurately predict *in vitro* noise, indicating that thermal noise dominates. In this paper, we demonstrate how broadband noise and impedance of the sputtered iridium oxide film (SIROF) UEA change when implanted in a real biological environment (rodent subject), finding an increase from approximately 10 nV/$\sqrt{\text{Hz}}$ to 30 nV/$\sqrt{\text{Hz}}$ in noise for frequencies <100 kHz. A low frequency excess noise source was also found below 1 kHz, which may be explained by biological background $1/f^2$ noise [6]. The work here contributes engineering-oriented characterizations meant to inform and improve neural interface design.

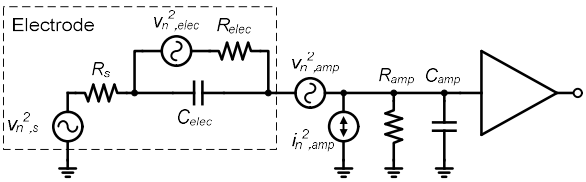


Fig. 1. Simplified electrode interface impedance and noise model.

## II. Electrode Noise and Impedance Characteristics

The noise and impedance of microelectrode arrays is known to vary between *in vitro* and *in vivo* conditions [7]. It is useful to leverage impedance data to predict electrode noise, as it allows cross-validation of noise and impedance measurements, but also because it is simpler to measure impedance than noise. Fig. 1 shows a simple electrode noise and lumped impedance (Randles) model. Low frequency impedance is dominated by the charge transfer resistance $R_{elec}$, but at higher frequencies, $R_{elec}$ is shorted by the double layer capacitance ($C_{elec}$) causing a flat high-frequency noise band from the series resistance of the electrode/tissue/solution interface ($R_s$). The electrode's thermal noise can be predicted from the impedance using (1) [8],

$$v_n^2(f) = 4kTRe[Z(f)] \quad (1)$$

where $v_n^2(f)$ is the voltage noise power spectral density, $k$ is Boltzmann's constant, $T$ is absolute temperature, and $Re[Z(f)]$ is the real part of the electrode impedance. If the electrode noise is mainly thermal, it will closely match the noise predicted using (1).

The magnitude of the electrode impedance is often cited at 1 kHz, but this unfortunately cannot describe the system noise. This motivates a spectral study of impedance and noise and their relationship. The *in vitro* experiments we presented in [5] provided wide-band characterization of impedance and noise. However, these measurements were acquired in an idealized saline environment. The current study uses (1) to understand noise in an implanted environment, and shows that under anesthetic that eliminates local cortical neuronal action potential activity (spiking) there is a strong correlation between measured noise and electrode impedance for the standard SIROF UEA.

## III. Methodology

Impedance data were collected using a Gamry Reference 600 Potentiostat. The spectral voltage noise of the electrode is fairly low level, and clean measurements thus require a custom printed circuit board (PCB) headstage as shown in Fig. 2. This headstage implements a two-stage wide-band voltage amplifier as shown in the figure. Our previous experiments [5] observed DC offset voltages as high as 150 mV across electrodes, so offset correction was applied to both circuit stages to prevent railing the amplifiers. In the first stage, $C_1$ is used to keep the DC gain at 1 V/V. The second stage uses an active DC servo loop to eliminate the DC offset, using $U_4$, $C_2$ and $R_6$ to set a high-pass filter corner. The PCB uses a multiplexer (ADG1206) at the input of the measurement chain to select each electrode. The multiplexer must be chosen such that the RC filter created by the input capacitance and total series resistance does not severely limit the measurement bandwidth.

Two versions of the custom headstage were required for high-accuracy noise measurements due to the intrinsic trade-off of $1/f$ voltage noise and input current noise [5]. The LT1793 JFET opamp was used at low frequencies for its low $1/f$ noise, but not above 25 kHz due to increased input current noise ($i_{n^2,amp}$). The LTC6244 was used at high frequencies because it has high $1/f$ noise but low $i_{n^2,amp}$. The measurement circuit's accuracy was verified using RC models of the electrodes.

### A. in vitro Characterization

Impedance measurements of a commercially available 4x4 (16 channel) UEA (Blackrock Microsystems) were taken using electrochemical impedance spectroscopy in PBS (0.150M NaCl, 0.016M $Na_2HPO_4$, 0.004M $KH_2PO_4$, pH 7.4) in a glass beaker using a two-electrode configuration with a platinum wire counter electrode. The Gamry Potentiostat was used to sweep a 20 $mV_{rms}$ sinusoid from 10 Hz to 500 kHz and to measure the resulting current.

Noise measurements were performed using the same PBS mixture and glass beaker. The custom headstage was attached to the UEA with a 16-pin A79016 Omnetics connector and data were recorded with a HP89441A spectrum analyzer. The noise voltage of the headstages ($V_{n^2,amp}$) was de-embedded from the electrode noise measurement by grounding both inputs and measuring $V_{n^2,amp}$, then subtracting the grounded-input measurement from the electrode measurement in post processing (MATLAB).

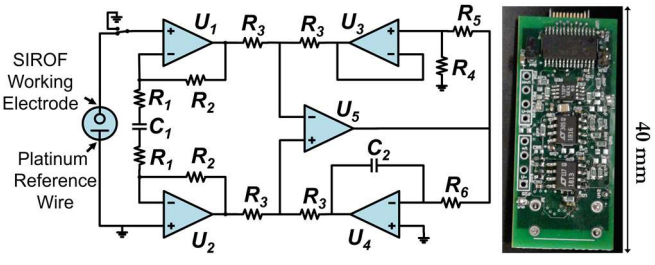


Fig. 2. Left: Simplified schematic of the noise measurement circuit. For $U_{1,2}$, GBW = 4.2 MHz (LT1793) or 50 MHz (LTC6244) and $A_{v1}$ = 32 (set by $R_1$, $R_2$). For $U_{3,4,5}$, GBW = 100 MHz (LT1813), $A_{v2}$ = 11 (set by $R_4$, $R_5$). The circuit uses +/- 2.5 V rails generated by 9 V batteries and linear regulators. Right: Custom PCB implementation of the noise measurement circuit.

### B. in vivo Characterization

The *in vivo* measurements were performed in a 472 g male Sprague Dawley rat. All studies were conducted with the approval of the Institutional Animal Care and Use Committee at the University of Utah. To induce anesthesia, the rat was placed in an induction chamber with a 5% volume of vaporized isoflurane and subsequently transferred to a nose cone system providing 0.5% to 5% isoflurane. The isoflurane percentage was adjusted over the course of the experiment in order to maintain a proper level of anesthesia, and has the effect of eliminating nearly all local spiking activity. The same UEA that was measured *in vitro* was sterilized and implanted in the left barrel cortex through a 4.5 mm diameter hole drilled in the cranium. A bone screw was placed into the temporal bone and a platinum ground wire (attached to the PCB ground) was secured to the bone screw. A second small hole was drilled posterior to the craniotomy and a platinum reference wire (tied to PCB ground) was inserted. All holes were filled with silicone and several layers of UV-cure epoxy were used to firmly secure the UEA, Omnetics connector, and wires.

A copper mesh Faraday cage was placed over the rat. The same headstages used for *in vitro* measurements were used in conjunction with the HP89441A to measure the noise from the implanted UEA. The Gamry potentiostat was used to measure the impedance using the reference wire as the counter electrode.

## IV. Results and Discussion

It is important to note that there are several layers of verification occurring here, in that the impedance and noise should correlate (at least *in vitro*) [5], and there are two custom headstages that have overlapping bandwidths from 1 kHz to 25 kHz. Data from both headstages match precisely in this overlap region, giving confidence to the overall measurement and de-embedding methodology. A comparison of the noise measured *in vivo* and *in vitro* is shown in Fig. 3. The *in vivo* noise voltage is found to be 2x to 3x higher compared to *in vitro*. The *in vivo* measured noise shows a significant increase below 1 kHz compared to the impedance and predicted thermal noise. This excess noise is possibly due to biological $1/f^2$ noise [6]. The *in vivo* measurements contain some high-frequency electromagnetic interference (EMI) due to the non-ideal experimental environment, likely coupling in through vital sign monitoring equipment. While these tones look significant, they are not distinguishable from the noise floor in the time domain.

The real part of the electrode impedance is the dominant noise source. Fig. 4 shows the measured impedance of the UEA

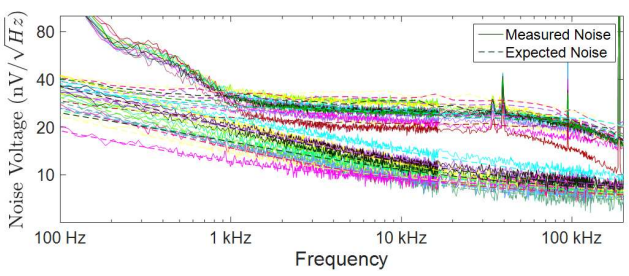


Fig. 3. Measured (solid) and expected (dashed) noise compared from 100 Hz to 200 kHz between *in vivo* (upper group) and *in vitro* (lower group) for 12 electrodes from the SIROF UEA.

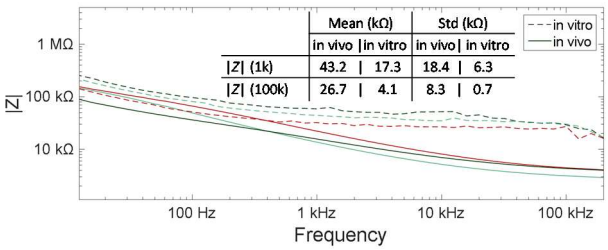


Fig. 4. Comparison of impedance magnitude from 10 Hz to 200 kHz *in vitro* (solid) and *in vivo* (dashed). Plots show only three selected electrodes for clarity, mean and standard deviation reported for all 12 electrodes.

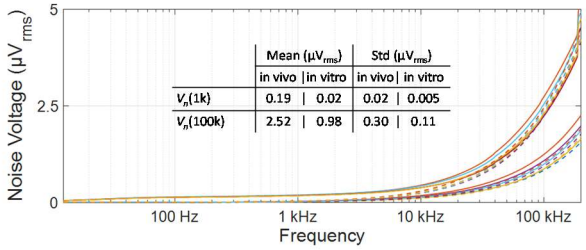


Fig. 5. Comparison of total integrated noise from 10 Hz to 200 kHz, *in vivo* (upper group) and *in vitro* (lower group). Dashed lines show expected thermal noise using (1), solid lines show measured integrated noise. Plots show only three selected electrodes for clarity, mean and standard deviation reported for all 12 electrodes.

*in vivo* and *in vitro*. The data show a significant increase in the *in vivo* impedance, leading to the increase in noise.

The total integrated noise is useful to know for circuit designers and is shown in Fig. 5, which compares the measured and predicted noise, *in vivo* and *in vitro*. Some minor abnormalities in the integrated noise can be seen at high frequencies for the *in vivo* measurements due to EMI. The effect of electrode implantation can be seen easily in the comparison of *in vitro* and *in vivo* measurements, i.e. the measured total integrated noise experiences a significant increase. Two main contributing factors are the corner frequency of the capacitive component shorting out $R_{elec}$ and an increase in $R_s$. The average *in vitro* integrated noise was measured to be 0.98 μVrms at 100 kHz, whereas the *in vivo* measurements (using the same electrodes) was measured to be 2.52 μVrms at 100 kHz.

The percent error between the measured and predicted *in vivo* noise demonstrates the reliability of using impedance measurements for predicting noise in a circuit design. Predicted noise matches within 20% for frequencies >1 kHz except for the influence of EMI, as shown in Fig. 6. This figure also shows that the total integrated noise error settles within 20% for most electrodes at high frequencies.

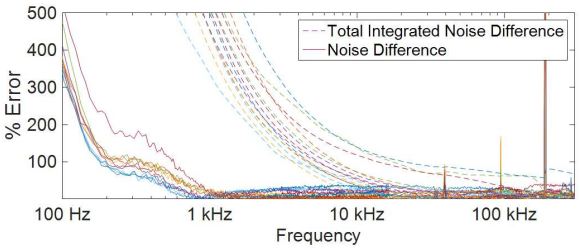


Fig. 6. Percent error between measured *in vivo* noise and predicted noise using (1) (solid) and total integrated noise error (dashed), for all 12 electrodes.

## V. Conclusion

This study built upon our previous work performing wide-band noise measurements of the SIROF Utah Electrode Array [5], and provides a comparison of noise characteristics *in vitro* and *in vivo*. This work has demonstrated excellent correlation between noise and impedance spectra in the well-controlled *in vitro* measurements, and has demonstrated a high degree of correlation in the high-frequency *in vivo* noise and impedance (matching within ~20% in mid and high-frequency regions). The low-frequency discrepancy may be accounted for by biological noise that is separate from the electrode noise itself. The noise across the measured bandwidth has been found to increase by a factor of 2x to 3x between *in vitro* and *in vivo*, increasing from approximately 10 nV/$\sqrt{\text{Hz}}$ to 30 nV/$\sqrt{\text{Hz}}$ at 10 kHz to 100 kHz.

These measurements are useful for the design of neural interfacing electronics and provide building blocks for understanding the wide-band characteristics of the electrode-tissue interface. Better understanding of this interface may lead to clues for failure modes and lifetime limitations of neural implants, and may provide a significant tool in the development of neural interface circuits and systems. The excess low-frequency noise warrants further investigation. A larger data set is also called for to compare *in vivo* data between more UEA devices as well as a comparative study of different array types.

## Acknowledgment

Thanks to L. Rieth, R. Caldwell and K. Bouchard for useful discussions, and to Linear Technology (now Analog Devices) for parts. This material is based upon work supported by the National Science Foundation Graduate Research Fellowship under Grant No. 1256065, and NIH 1R21EY027618-01.

## References

[1] F. Willett, C. Pandarinath, B. Jarosiewicz, B. Murphy, W. Memberg, C. Blabe, et al., "Feedback control policies employed by people using intracortical brain–computer interfaces," Journal of Neural Engineering, vol. 14, no. 1, p. 016001, 2016.

[2] B. Gunasekera, T. Saxena, R. Bellamkonda and L. Karumbaiah, "Intracortical recording interfaces: Current challenges to chronic recording function," ACS Chemical Neuroscience, vol. 6, no. 1, pp. 68-83, 2015.

[3] W. Franks, I. Schenker, P. Schmutz, and A. Hierlemann, "Impedance characterization and modeling of electrodes for biomedical applications," IEEE Trans. Biomed. Eng., vol. 52, no. 7, pp. 1295–302, Jul. 2005.

[4] K. P. Koch, M. Schuettler, and T. Stieglitz, "Considerations on noise of electrodes in combination with amplifiers for bioelectrical signal recording," Biomed. Tech. Eng., vol. 47, pp. 514–516, 2002.

[5] M. Sharma, A. T. Gardner, J. Silver and R. M. Walker, "Noise and impedance of the SIROF Utah Electrode Array," 2016 IEEE Sensors, Orlando, FL, 2016, pp. 1-3.

[6] J. Milstein, F. Mormann, I. Fried and C. Koch, "Neuronal shot noise and Brownian 1/$f^2$ behavior in the local field potential," PLoS ONE, vol. 4, no. 2, p. e4338, 2009.

[7] X. Wei, W. Grill, "Impedance characteristics of deep brain stimulation electrodes in vitro and in vivo," Journal of Neural Engineering, vol. 6, no. 4, p. 046008, 2009.

[8] H. Nyquist, "Thermal agitation of electric charge in conductors," Phys. Rev., vol. 32, p. 110, 1928.